





## Original Article

## Morphodynamics and sediment connectivity index in an unmanaged, debris-flow prone catchment: a through time perspective

Loris TORRESANI<sup>1</sup>  <https://orcid.org/0000-0003-2830-6792>;  e-mail: [loris.torresani@phd.unipd.it](mailto:loris.torresani@phd.unipd.it)

Guillaume PITON<sup>2</sup>  <https://orcid.org/0000-0002-0124-0909>; e-mail: [guillaume.piton@inrae.fr](mailto:guillaume.piton@inrae.fr)

Vincenzo D'AGOSTINO<sup>1</sup>  <https://orcid.org/0000-0003-2261-9069>; e-mail: [vincenzo.dagostino@unipd.it](mailto:vincenzo.dagostino@unipd.it)

\*Corresponding author

<sup>1</sup> Department of Land, Environment, Agriculture and Forestry, University of Padova, Agripolis, Viale dell'Università 16, 35020 Legnaro (PD), Italy

<sup>2</sup> Université Grenoble Alpes, INRAE, CNRS, IRD, Grenoble INP, IGE, 38000 Grenoble, France

**Citation:** Torresani L, Piton G, D'Agostino V (2023) Morphodynamics and sediment connectivity index in an unmanaged, debris-flow prone catchment: a through time perspective. *Journal of Mountain Science* 20(4). <https://doi.org/10.1007/s11629-022-7746-2>

© The Author(s) 2023

**Abstract:** Torrential processes are among the main actors responsible for sediment production and mobility in mountain catchments. For this reason, the understanding of preferential pathways for sediment routing has become a priority in hazard assessment and mitigation. In this context, the sediment Connectivity Index (IC) enables to analyse the existing linkage between sediment sources and the selected target (channel network or catchment outlet). The IC is a grid-based index that allows fast computation of sediment connectivity based on landscape information derived from a single Digital Terrain Model (DTM). The index computation is based on the log-ratio between an upslope and a downslope component, including information about drainage area, slope, terrain roughness, and distance to the analysis target (e.g. outlet). The output is a map that highlights the degree of structural connectivity of sediment pathways over analysed catchments. Until now, these maps are however rarely used to help defining debris-flow hazard maps, notably due to a lack of guidelines to interpret the IC spatial distribution. This paper proposes an exploitation procedure along profiles to extract more information

from the analysis of mapped IC values. The methodology relies on the analysis of the IC and its component variables along the main channel profile, integrated with information about sediment budgeting derived from Difference of DEMs (DoD). The study of connectivity was applied in the unmanaged sub-catchment (without torrent control works) of the Rio Soial (Autonomous Province of Trento – NE Italy) to understanding the geomorphic evolution of the area after five debris flows (in ten years) and the related changes of sediment connectivity. Using a recent DTM as validation, we demonstrated how an IC analysis over the older DTM can help predicting geomorphic changes and associated hazards. The results show an IC aptitude to capture geomorphic trajectories, anticipate debris flow deposits in a specific channel location, and depict preferential routing pathways..

**Keywords:** Sediment Connectivity Index; Debris flow; Hazard assessment; Digital Elevation Model; Geomorphic evolution; DEMs of Difference

### 1 Introduction

In alpine regions, the understanding of sediment

**Received:** 03-Oct-2022  
**Revised:** 06-Jan-2023  
**Accepted:** 24-Mar-2023

yield and delivery from hillslopes to channels is crucial during hazard assessment and mitigation planning. Torrential processes such as debris flows, debris floods, and landslides are key actors in relocating sediment, thus shaping an alpine catchment (Benda et al. 2003; Korup et al. 2010; Mao et al. 2009; Schneuwly-Bollschweiler and Stoffel 2012). Debris flows (DF) are considered among the most dangerous natural hazards in mountain areas, capable of dramatic geomorphic changes. The composition of a DF is characterised by a mixture of boulders, sediment, water and air (Kaitna and Huebl 2013; Takahashi 1981) with a solid volumetric concentration that ranges from 25% to 70% (Costa and Williams 1984; Takahashi 1981).

In a debris flow-prone catchment, erosion usually occurs in the upper part of the catchment, where the slope gradient and confinement are usually high (Gregoretti et al. 2019), or along hillslopes close to an active channel. Then, slope and confinement usually decrease as approaching the fan apex, causing the debris flow to spread and deposit part of the transported sediment. The fan areas, or where confinement and slope drops, are morphologically shaped by a sequence of autogenic avulsions, local incisions and sediment relocation (De Haas et al. 2016; Kumar et al. 2019; Reitz and Jerolmack 2012). Therefore, a better understanding of geomorphic evolution is essential in debris flow prone catchments to predict the response to climate change and anticipate possible degradation trends (Lane 2013).

Capturing the geomorphologic evolution of a mountain catchment has recently been improved by employing modern and cost-effective remote sensing techniques (Agüera-Vega et al. 2018; Ghuffar 2018; Tarolli 2014). One of the most effective methods to obtain a high-resolution Digital Terrain Model (HR-DTM) is the use of Remotely Piloted Aircraft Systems (RPAS) and the application of the Structure from Motion (SfM) and Multi-View Stereo (MVS) techniques. The availability of multi-epoch DTMs enables geomorphic changes to be analysed at pixel size by computing a Difference of DEMs (DoD). Furthermore, the computation of a DoD allows sediment budgeting to be obtained at a low cost (Cavalli et al. 2017; Cucchiario et al. 2019; Williams 2012). Detailed catchment-scale topography enables flow and sediment paths to be analysed more accurately with different approaches or numeric models.

Identifying sediment sources, and how they are linked with the channel network, is relevant to tailor an effective hazard mitigation plan. In particular, in situations where sediment delivery from sediment sources moves through massive movements, causing adverse effects on the environment and human infrastructures (D'Agostino and Bertoldi 2014; Lane et al. 2007). The determination of connectivity (i.e. the degree in which water and sediment are prone to be transferred from a catchment point to another) and disconnectivity (i.e. the degree of constraint on sediment transfer by any limiting factor) can characterise how the sediment conveyor belt works during rainstorm events. This global understanding can help integrate the knowledge to enhance hazard mitigation planning (Fryirs 2013).

Many innovative indices and models were introduced to describe sediment connectivity on different spatial scales (Borselli et al. 2008; Cavalli et al. 2013; Heckmann et al. 2018; Heckmann and Schwanghart 2013; López-Vicente et al. 2015; Messenzehl et al. 2014; Najafi et al. 2021). The same authors identify two types of connectivity: "direct connectivity" via channels or gullies and "diffuse connectivity" as overland flow paths down the slope to the stream network. Another classification is proposed by Brierley et al. (2006), in which the connectivity is grouped into vertical, longitudinal and lateral. A connectivity analysis also includes identifying geomorphic features that promote disconnectivity, helping to capture the reduction in sediment delivery efficiency across the catchment (or channel network) (Fryirs et al. 2007). Blockages are geomorphic features that inhibit the natural continuity of longitudinal and lateral connectivity. Longitudinal connectivity (upstream to downstream connection) can be inhibited by "barriers" like bedrock steps, woody debris or check dams that change the local level of the channel bed (Fryirs et al. 2007). Lateral connectivity (hillslope to stream) can be limited by the presence of the so-called "buffer", which can be represented by alluvial pockets or fans (Harvey 2001).

One of the widely used geomorphic indexes to quantify sediment connectivity is the Connectivity Index (IC) proposed by Borselli et al. (2008), later modified for alpine catchments by Cavalli et al. (2013). A connectivity analysis using the IC allows describing the preferential sediment paths and the structural connectivity computed at pixel scale from hillslopes to

a user-defined target (i.e. outlet or channel network). The actual computation is based on a log-ratio of an upslope and a downslope component derived from a single DTM. These two components include information about the topography, surface roughness, and land use (Heckmann et al. 2018; López-Vicente and Ben-Salem, 2019). The IC has proven its effectiveness in different environments and study objectives (Cucchiaro et al. 2019; Masselink et al. 2016; Ortíz-Rodríguez et al. 2017; Pellegrini et al. 2021; Schopper et al. 2019; Zhao et al. 2020).

There is still scarce information about IC's predictive and descriptive capability about the geomorphic evolution of a debris flow channel. In the present work, a particular disconnectivity of sediment transfer is reported, and it is related to flow spreading (or autogenic channel avulsion) over fan areas. This can happen due to a decreased channel confinement and slope that promotes sediment deposition by the flow.

This paper presents a combination of methods for understanding the geomorphic evolution of a debris flow channel and the influence on the sediment connectivity index in a small alpine sub-catchment. The working hypotheses are that (H1) through time changes in IC can help to consolidate geomorphic evolution on current and short-term geomorphic trajectories and that (H2) trends of debris flow channel evolution towards erosion or deposition are correlated to sediment connectivity and should appear in the IC analysis. By looking in detail at the spatial changes of the various parameters involved in the IC computation, this work also seeks to give insights on the underlying mathematics leading to an IC map, which will be useful to interpret it. It could be considered to be a degradation of the approach to come back to a 1D analysis while 2D, 3D and 4D (3D + time) are becoming the standard. On the contrary, we believe that we help consolidating the use and interpretation of more complex data by analysing how an integrated index as the IC is really computed.

Here we verify how a longitudinal analysis can integrate the derived knowledge from a spatial analysis of the connectivity index. The basic approach proposed uses a single epoch DTM to predict the potential geomorphic evolution through an integrated IC analysis approach. Then, post-event data help corroborate IC analysis predictions by a DTM differencing analysis (DoD computation) and validate H1. This provides the future geomorphic trajectory that the system may follow (Rinaldi et al. 2011). The

paper first presents the study area and methods used in the analysis. Secondly, it provides a concise typical debris-flow channel assessment and highlights the insights gained by the new analysis. Lastly, the potential of this integrative procedure to enrich debris-flow hazard analyses is discussed.

## 2 Material and Methods

### 2.1 Study area

The study area is a small sub-catchment of the Rio Soial watershed located in the municipality of Sèn Jan di Fassa, in the eastern part of the Autonomous Province of Trento – North-East Italy. The watershed drainage area is 17.2 km<sup>2</sup> and ranges from 1678 m a.s.l. to 3002 m a.s.l. at the "Catinaccio d'Antermoia" peak, with an elevation drop of 1324 m. The main channel is the "Rio Soial", and it is about 4000 m in length from the source to its confluence with the Avisio Torrent. This area falls entirely within the Rosengarten-Catinaccio massif of the Dolomites (ISMSA code: II/C-31.III-B.8) and is recognised as a UNESCO World Heritage Site. The geology is mainly composed of Breno formation and Scillar's dolomite of the Anisian and Carnian periods.

The vegetation is composed of red fir (*Picea Abies*) forests below approximately 1900 m a.s.l., dwarf pine (*Pinus Mugo*) from 1900 m a.s.l. to 2100 m a.s.l., and alpine shrubland (*Rhododendron hirsutum*) above 2100 m a.s.l. The average annual precipitation is 800 mm and occurs mainly in short but intense rainstorms in summer (July and August).

The analysis focuses on a small sub-catchment of the Rio Soial, located in the south-western part of the catchment (Fig. 1). This sub-catchment has a drainage area of 0.54 km<sup>2</sup>. The main channel length is 1900 m and drops from 2566 m a.s.l. at "Passo dei Mugoni" to 1928 m a.s.l. at the confluence with the "Rio Soial" (Latitude 46.44695; Longitude 11.64181 - WGS84 ). The channel is ephemeral, with water flowing only during moderate to high-intensity rainstorms or in spring due to snow melting. The valley morphology is "V-shaped" with steep and unstable slopes, which play a very active role in sediment delivery to the channel bed (Fig. 2). Due to this high sediment availability from the steep slopes, this sub-catchment can be considered sediment supply-unlimited (or transport limited) (Bovis and Jakob 1999).

Two DTMs are available and cover a ten years period. The first DTM derives from a lidar flight operated during October 2008 (commissioned by the Autonomous Province of Trento), and the second one derived from an RPAS flight performed in July 2018.

Within this interval, the Mountain Basin Service of Trento recorded five debris flow events. For each event, technical reports indicate the typology of the phenomena and a gross damage description. In July 2019 (not covered by the available dataset), a debris

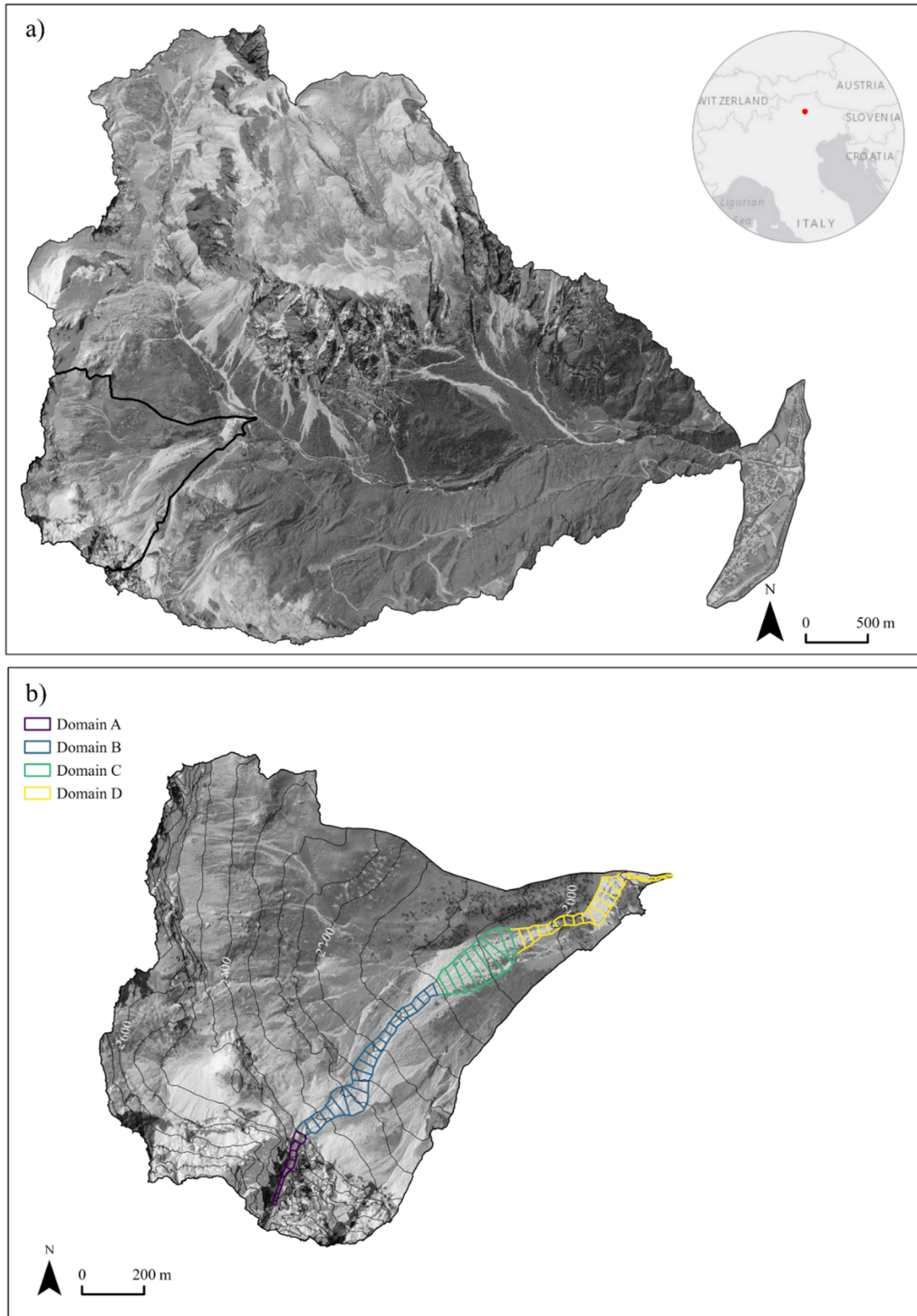


**Fig. 1** a) Maps of the entire Rio Soial catchment, including the urbanised alluvial fan, b) analysed sub-catchment with unstable debris flow channel. Subchannel position is highlighted with the black border.

flow occurred on the channel under study, and one at a channel located few hundred meters along the eastern direction (outside the study area). The triggered debris flows partially hit private cottages, a mountain hut, and the active grazing land, causing moderate damage.

The sub-catchment is visited by many tourists and sports enthusiasts that cross the fan area due to the presence of alpine tracks to the local summits. For these reasons, the understanding and monitoring of debris flow dynamics here has become of high priority.

## 2.2 Debris flow channel analysis

The study area was first studied using satellite

imagery (current and past), DTMs (hillshade interpretation), and field surveys to better understand its characteristics. Imagery and field visits enabled mapping sediment source areas, understanding the varied geological setting (transition from bedrock channel to talus slopes), and identifying geomorphic characteristics (slopes, channel depth and width, evidence of past events). This preliminary phase concluded with the identification of several homogeneous reaches in the channel hereafter called “domains”: (A) Narrow confined and steep channel, (B) Incised channel on talus slope, (C) Upper fan, (D) Fan distal part and rangeland (Fig. 1b).



**Fig. 2** Photos of the channel: a) upper part of the basin - domain A, b) deep incised channel – domain B, c) final part of the incised channel – domain B, d) upper fan area where flow spreading is predominant – domain C, e-f) rangeland and paved channel to the confluence with the Rio Soial – domain D. (the white arrow indicates the flow direction).

### 2.3 Preliminary analysis and scale of investigation

The analyses performed in this work were based mainly on digital terrain models (DTM) and post-processing in a GIS environment. The available datasets of the catchment were a 1 m resolution LiDAR-derived DTM from the 2008 flight, and a 1 m resolution UAV-derived DTM of the sub-catchment area performed in July 2018. The LiDAR DTM is characterized by a point cloud mean density of 1.28 point/m<sup>2</sup> with an average point spacing of 0.9 m (Ufficio Sistemi Informativi - Servizio autorizzazioni e valutazioni ambientali 2009). The second DTM was generated from an RPAS-derived point cloud. The point number was about 67 million points with a mean density of about 400 points/m<sup>2</sup>.

The first step focuses on choosing the most appropriate scale (pixel resolution) to produce the analyses (Hengl 2006). This is essential since the resolution choice affects the outputs and interpretation of the results.

The analysis has to be chosen according to the geomorphic phenomena under study. Thus, it is essential to evaluate the scale of the torrential process, knowing its physics and the morphology of the selected channel network. The task included several trials using various resolutions (in the range 1-10m) before choosing the most appropriate scale for obtaining a clean output. The combination between channel morphology (mean width and confinement) and the willingness to focus only on morphological characteristics relevant to debris flow led us to choose a 5 m pixel resolution. By doing this, it has been possible to retain landforms that are more appropriate to describe the main morphological marks of a debris flow channel in mountain catchments (gullies, lobes, paleo-channels). Moreover, the proper pixel size choice avoided including micro-topography features that would be useful in a numerical flow spreading simulation, but would produce noisy outputs in an IC analysis. It would include details irrelevant to debris flow dynamics that would rather be relevant for low runoff. Another motivation for choosing the appropriate resolution choice is understanding and analysing significant flow paths, especially where flow dispersal predominates.

### 2.4 Application of Sediment Connectivity Index

The assessment of sediment connectivity was based on applying the geomorphic-based index proposed by Cavalli et al. (2013). The sediment connectivity analysis relies on potential sediment route tracing from hillslope to a user-defined target. An IC target can be the channel network for lateral connectivity assessment or the catchment outlet to compute the overall catchment connectivity, and it is computed by Eq. 1. The equation defines the IC as the log<sub>10</sub> ratio between (i) an upslope component ( $D_{up}$ ), which is the product of the square root of the catchment area, the mean slope of this drainage area and a mean value of upslope weighting factor on the same drainage area; and (ii) a downslope component ( $D_{down}$ ), which is the sum of the distance to the downstream sink divided by the weighting factor and slope of each pixel. The IC ranges theoretically within the interval  $[-\infty, +\infty]$  and increases as connectivity with the sink increases. In the present study area IC ranges between -4 and -2.5, and it is comparable to values found over alpine catchments (Cavalli et al. 2013; Tarolli and Sofia 2016).

$$IC_k = \log_{10} \left( \frac{D_{up}}{D_{down}} \right) = \log_{10} \left( \frac{\overline{W}_k \overline{S}_k \sqrt{A_k}}{\sum_{i=k, \dots, n_k} \frac{d_i}{W_i S_i}} \right) \quad (1)$$

With  $k$  = pixel index for which IC is computed,  $W_i$  = weighting factor of the pixel  $i$ ,  $\overline{W}_k$  = mean value of  $W_i$  on all pixels belonging to the contributing area of pixel  $k$ ,  $S_i$  = slope of pixel  $i$ ,  $\overline{S}_k$  = mean value of  $S_i$  on all pixels belonging to the contributing area of pixel  $k$ ,  $A_k$  = drainage area of pixel  $k$ ,  $k, \dots, n_k$  = are the indexes of all pixels on the path from pixel  $k$  to the target, and  $d_i$  = distance of path in pixel  $i$ .

“The IC computation for steep mountain catchments proved to be more relevant by Cavalli et al. (2013) when (i) bounding slopes in the range 0.5%-100% to focus on torrential flows and prevent bias related to near vertical points or flat areas in the DTM, and (ii) computing the contributing area with an algorithm that accommodates flow spreading on pixels with low elevation difference rather than artificially concentrating flow in one single lower pixel (D-infinity algorithm as defined by Tarboton 1997)”.

The weighting factor ( $W$  - unitless) was first introduced by Borselli et al. (2008) to include the resistance to water flows in the model. The estimation of this factor is based on the USLE-RUSLE Cover Management factor (C-factor), which describes local land use conditions. The weighting factor can be computed from analysing different features, allowing the user to fit different analysis needs and landscape

settings by choosing the proper impedance factor ( $W$ ). Some of the impedance factors that can be used are the C-factor of USLE-RUSLE, the SCS-CN, Manning's  $n$ , and the Topographic Roughness Index (Borselli et al. 2008; Cavalli et al. 2008; Llana et al. 2019; Martini et al. 2020; Zanandrea et al. 2020). Due to the typical alpine context of the presented study area, the normalised topographic roughness index (RI) was reported to be the most appropriate indicator to depict water flows impedance (Trevisani and Cavalli 2016). This choice was also supported by the absence of relevant vegetation or human land-use alterations.

The RI (Eq. 2 - Cavalli et al. 2008) is computed as the standard deviation of the residual topography obtained by subtracting a smoothed version of the DTM from the original.

$$RI = \sqrt{\frac{\sum_{i=1}^{25} (x_i - x_m)^2}{25}} \quad (2)$$

where 25 is the number of computing cells inside the moving window ( $5 \times 5$  cells),  $x_i$  is the value of the residual topography for one specific cell, and  $x_m$  is the mean value of residual topography of all 25 cells.

The computation of the roughness index derived weighting factor requires a 0 to 1 normalisation by natural logarithm, according to Eq. 3. The logarithm normalization aims to overcome the compression of variability when using the linear normalization of RI on mountain environments, as proposed in the original concept by Borselli et al. (2008).

$$W = 1 - \frac{\ln(RI) - \ln(RI_{\min})}{\ln(RI_{\max}) - \ln(RI_{\min})} \quad (3)$$

$RI_{\max}$  and  $RI_{\min}$  are the maximum and minimum RI, trimmed to 0.001 to avoid  $W_i=0$  in the computation of the downslope component (Cavalli et al. 2013).

Computation of the IC was performed using the SedInConnect application (Crema and Cavalli 2018). This tool allows the IC to be evaluated at pixel size with a fast and flexible workflow, requiring only a DTM as input and few options to customise the analysis. In addition, a shapefile to define the analysis target (confluence with the Avisio river) has been provided to compute the index regarding this section of the study area.

The toolbox allows the IC calculation by using a custom "W" or choosing the RI automatic procedure. There is also the option to use the normalisation proposed by Trevisani and Cavalli (2016), according to Eq. 3. Computing the RI over a  $5 \times 5$  cell moving window directly over the 5 m DTM would cause a

surface over smoothing over a  $625 \text{ m}^2$  moving window, and this will cause a loss of details and a poor roughness description. So, the solutions are mainly two. The first one is to adjust the moving window size considering the feature dimensions to investigate and the resolution of the DTM.

The second solution, which was used in this case, is possible thanks to the availability of higher resolution DTM, is performing the first iteration of SedInConnect using the 1 m DTM thus getting a sub-grid scale information. In this way, the moving window size is  $25 \text{ m}^2$  and describes a local surface roughness from a high-resolution source. Consequently, the derived  $W$  is computed on a more appropriate scale for roughness analysis in debris flow prone channels, highlighting the presence of smooth or highly confined morphologies. Finally, an aggregation by averaging resolution from 1 m to 5 m then allowed the production of a custom weighting factor to be used in the second iteration of SedInConnect for the final assessment of IC.

The pixel-based analysis of sediment connectivity was conducted in the sub-catchment utilising the Index of Connectivity to analyse the longitudinal connectivity, i.e. from headwater to catchment outlet. We aimed to understand sediment connectivity in the sub-catchment domain to visually interpret how IC has detected confinement and geomorphic conditions of each homogeneous segment.

## 2.5 Profile analysis of Sediment Connectivity Index

To provide an alternate perspective on IC outputs, the procedure we propose relies on an analysis of IC and its components in debris flow prone catchment along selected profiles. The procedure is mainly based on the extraction of each variable that composes the IC along a point sampling profile of the selected watercourse. Sampling points were derived from the flow accumulation raster of the investigated sub-catchment: a flow accumulation threshold was sought to identify the starting points of channels, and the channel network was delineated starting from these points. A "raster to point" conversion produced the profile required for the next steps of the analysis. The extraction from the flow accumulation raster implies including the evolution and changes of the thalweg profile when using multi-temporal DTMs. It must be stressed that when performing such an analysis on

different DTMs, the axis of the profile may change because of shifting and eventual avulsion of the axis of the main channel. Such a cut-off or on the contrary sort of meandering might reconnect or disconnect the whole system, which was interesting to point out. That is why we preferred this option to the alternative choice of considering arbitrarily that the channel should be considered along one given axis and that other flow paths would be irrelevant in our analysis.

We segmented 30 m-long reaches of the active channel to analyse variables at reach scale. The operations of mapping and segmentation were supported by using the semi-automatic ArcGIS toolbox “RiverCorridor”, developed by Roux et al. (2015). Before creating the final reaches shapefile, a visual inspection and manual editing of the features assured the highest accuracy of riverscape mapping. Finally, reaches were grouped into four homogeneous domains according to confinement degree (O’Brien et al. 2019) and common geomorphic characteristics. The computation of reach-averaged values employs two methods. The first is based on performing the sum of each pixel value of the DoD located within each polygon (to derive the net erosion/net deposition) and then divide the result by the reach surface to compute an reach-averaged erosion or deposition depth  $\Delta Z$ . The second is based on a mean estimation derived from the sampling point within each reach to compute reach-averaged IC or other parameter.

The variables extracted along profile are the Connectivity Index (IC), Roughness Index (RI) and the derived Weighting factor ( $W$ ), Upslope component ( $D_{up}$ ), Downslope component ( $D_{down}$ ), Slope ( $S$ ), Contributing Area ( $A$ ) and sediment budgeting ( $\Delta Z$ ) derived from DTM differencing (DoD).

A detrended Index of Connectivity (DetIC) was introduced by a non-linear model fitting of IC values. In this way, it has been possible to compute a detrended IC without the influence of distance to the outlet. The upslope component has been filtered to discard the effect induced by the natural increase of drainage area from source to the outlet to highlight better the flow-spreading dynamic automatically computed within the IC framework. Thus, a detrended upslope component (DupDet) production allows changes induced by flow spreading in the selected flow path to be better discerned. The extraction of each variable value into a text file was performed using a data sampling algorithm available

ArcGIS Pro 2.5.1 (or QGIS).

Finally, we produced an R script to manage and process all the extracted values in the study area, including the computation of the detrended IC. This R code evaluated the IC components and their interaction to geomorphic settings in a fast and semi-automatic way. A further description of the methods and an integrated R tool (called R\_IC) is also reported in (Baggio et al. 2022; Martini et al. 2022).

## 2.6 Geomorphic evolution assessment and connectivity changes

The assessment of geomorphic changes is based on comparing at least two DEMs representing the geomorphic status of two different epochs on a Difference of DEM (DoD) elaboration. This operation operates a pixel-basis the elevation difference of overlapping pixels, computing sediment budgeting as volumetric balance.

The quality of a DoD depends mainly on the quality of the two DTMs, so it is fundamental to perform a proper uncertainties analysis to discriminate real changes from noise and artefacts.

The method used here is based on the concept proposed by Wheaton et al. (2010) for the estimation of a spatially uniform minimum Level Of Detection (minLOD) using Eq. 4:

$$\text{minLOD} = t \sqrt{\text{SDE}_{2018}^2 + \text{SDE}_{2008}^2} \quad (4)$$

SDE is the standard deviation of the error computed from the difference between DGPS measured Ground Control Point (GCP) elevation and the value extracted from the 2008 and 2018 DTMs. “ $t$ ” is the critical t-student’s value at a chosen confidence interval (in this work, 1.96). To produce the DoD of the analysed sub-catchment, the minLOD was set at 0.33 m.

The elaboration and thresholding of the DoD were performed using the standalone version of Geomorphic Change Detection 7 (GCD 7). This toolbox allows the volume budgeting of erosion/deposition in a selected study area to be computed. As integrative data, some representative cross-sections of each domain are reported in the results section.

Thus, visual interpretation of maps, combined with the novel quantitative analysis of connectivity, will help to improve the knowledge about geomorphic changes in the sub-catchment.



### 3 Results

#### 3.1 Identification of main geomorphic domains

The domains identified in the studied sub-catchment are reported in Fig. 1b and Fig. 2. In addition, a summary table (Table 1) reports some main features of the channel and the criteria used to determine the boundary between them. In essence, the studied area is a typical debris flow sub-catchment with very steep headwaters within the source areas and talus slopes where the channel is confined as a

gully (Domains A and B). The hillslope toe being composed of a debris fan with a wider channel where flow spread and debris tend to deposit (Domain C) before being reworked by surface runoff and bedload transport (Domain D).

#### 3.2 Application of Sediment Connectivity Index

The IC analysis allows the most potential sediment pathways to be depicted through a spatially distributed index on maps. Observing the outputs, the

**Table 1** Basic geomorphic parameters that define each homogeneous domain.

Domain	Slope (m/m)	Channel width (m)	Reach length (m)	Melton Index (-)	Confinement	Downstream boundary
A	-0.63	20.9	264	1.47	Yes	Transition from bedrock to talus slope
B	-0.47	24.3	633	2.03	Yes	Transition from incised channel to flow spreading area
C	-0.19	73.7	316	2.85	No	No more debris flow lobe spread on the fan
D	-0.17	28.5	619	0.85	Partial	Confluence with Rio Solal

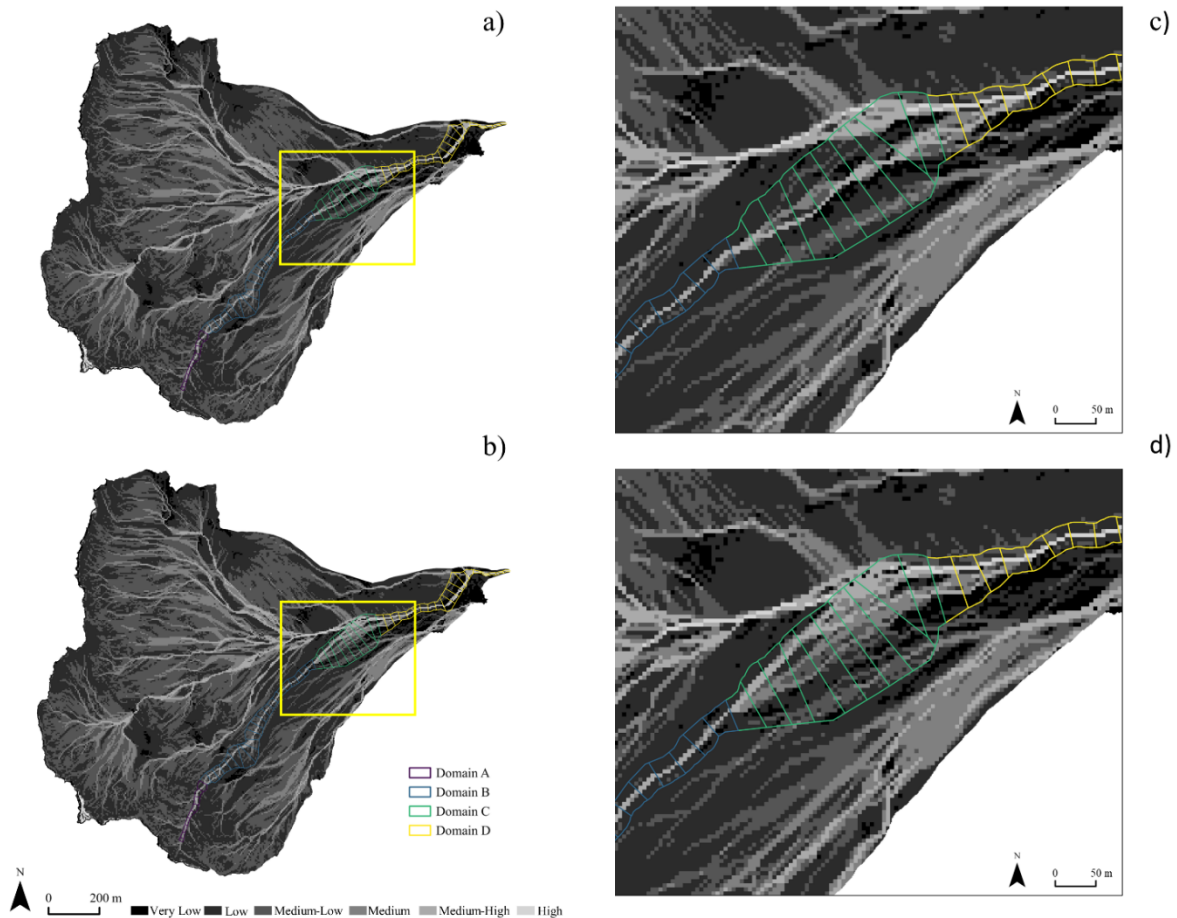


**Fig. 3** Maps of Connectivity Index: a) - (c) in 2008 and b) - (d) in 2018. Evidence of changes in the flow path in the downstream deposition areas (domain C). However, it is not easy to compare differences with only a visual interpretation of maps.

index follows a constant rise of the value along preferential pathways caused by the simultaneous increase of drainage area and the reduction of the distance to the outlet. The trend is observable in IC applications (Fig. 3a – 2008; Fig. 3b - 2018).

The high IC of the stream network reflects the high probability of delivering sediment from sediment source areas near the streams to the catchment outlet. Moreover, mapped IC values also help identify flow spreading areas in this specific case in the fan area (Fig. 3a-3b; within domain C) and how its magnitude has increased due to deposition and avulsion dynamics caused by the debris flows between the two epochs.

More in detail, we observed a low flow spreading in the 2008 IC (Fig. 3a) with a clear presence of a very connected channel. It is also possible to observe a channel merging in domain D.

Conversely, in the 2018 application of IC, the flow spreading degree in domain C has increased (Fig. 3b), explaining the higher number of moderately connected channels. There is also the evident absence of highly connected channels, and a channel merging in domain C.

### 3.3 Longitudinal exploitation of Connectivity Index factors

This section will report the results as IC plots along the thalweg, from the overall perspective to relevant sections (Fig. 3). The parameters included in the plots are, for each pixel  $k$ : elevation  $Z_k$ ,  $IC_k$  (with non-linear fitting), the local Weighting factor  $W_k$ , drainage area  $A_k$ , detrended Upslope component  $\overline{W}_k * \overline{S}_k * \sqrt{A_k}/\sqrt{A}$ , i.e., detrended from increases of the drainage area and Downslope component  $\sum_i d_i/W_i S_i$ .

The profile analysis of IC (and related components) showed different patterns in the sub-catchment domains. The resulting plots of the 2008 DTM analysis show how each analysed factor behaves along the thalweg profile. Figure 4c reports the computed IC profile and non-linear fitting of the IC (grey line). Regarding IC values, the longitudinal analysis shows values close to the trend in the confined area of the channel (domains A and B).

Conversely, IC tends to be more variable in the fan area (domain C) and in the first part of domain D, where channel confinement is lower. Flow channelling then becomes more evident, increasing confinement and subsequently stabilising IC close to the non-linear model. However, some IC

perturbations are visible, especially at the beginning of domain B (just after the end of the bedrock outcrop section). Here, the flow splits into two channels (Fig. 4e), inducing a decrease of IC and thus a less efficient transport capacity. Another evident perturbation of IC is observable between domain C (fan area) and the beginning of domain D. Here, the IC values remain stable around the -3.5 value (with local drops). Like the previous case, the flow spreading in fan areas and on a smooth surface is the main driving factor that leads the IC to drop below the fitted model. The sudden increase of IC in domain D is related to the channel merging, with a subsequent increase of drainage area and transport capacity. So the transport capacity became higher and prone to deliver sediment to the downstream areas (pastureland and mountain hut).

As integration to what was reported in the visual analysis of IC (section 3.1), it is immediately observable how the drainage area plot (Fig. 4b) efficiently identifies the exact point in which channel merging happens in domain D (Fig. 4b).

Performing a longitudinal analysis of all IC computation factors provides insight into how geomorphic evolution leaves a mark inside the analysed components. The signs of perturbation of IC are also observable in the area detrended Upslope component (Fig. 4e, as  $\overline{W}_k * \overline{S}_k * \sqrt{A_k}/\sqrt{A}$  or DupDet). Drops of IC at the beginning of domain B are reflected by DupDet drops (around the value of 0.25) and for a similar length. The same is observable for the perturbation of connectivity in domains C and D, where DupDet shows frequent drops to low values (from 0.3 to 0.1). As to the IC perturbation detected in the 2008 DTM analysis, it is possible to expect more deposition due to lower functional connectivity in these areas. Then, the 2018 DTM analysis aims to validate predictions made over the 2008 analysis and deliver insights on what to expect in the future.

The weighting factor plot (Fig. 4d) shows a wide fluctuation of values according to the roughness degree of the thalweg. Generally, in domains A and B, the values of  $W$  range around  $0.54 \pm 0.03$ ,  $0.55 \pm 0.04$ , respectively. These values display a rougher surface in the non-confined part of the channel. Domain C and D show  $W$  values of  $0.58 \pm 0.04$  and  $0.61 \pm 0.05$ , respectively (Table 2). However, when referring to landform relief, the roughness index (RI) is more appropriate for describing surface characteristics since it is not affected by the normalisation needed to obtain the  $W$  factor (if the behaviour remains the

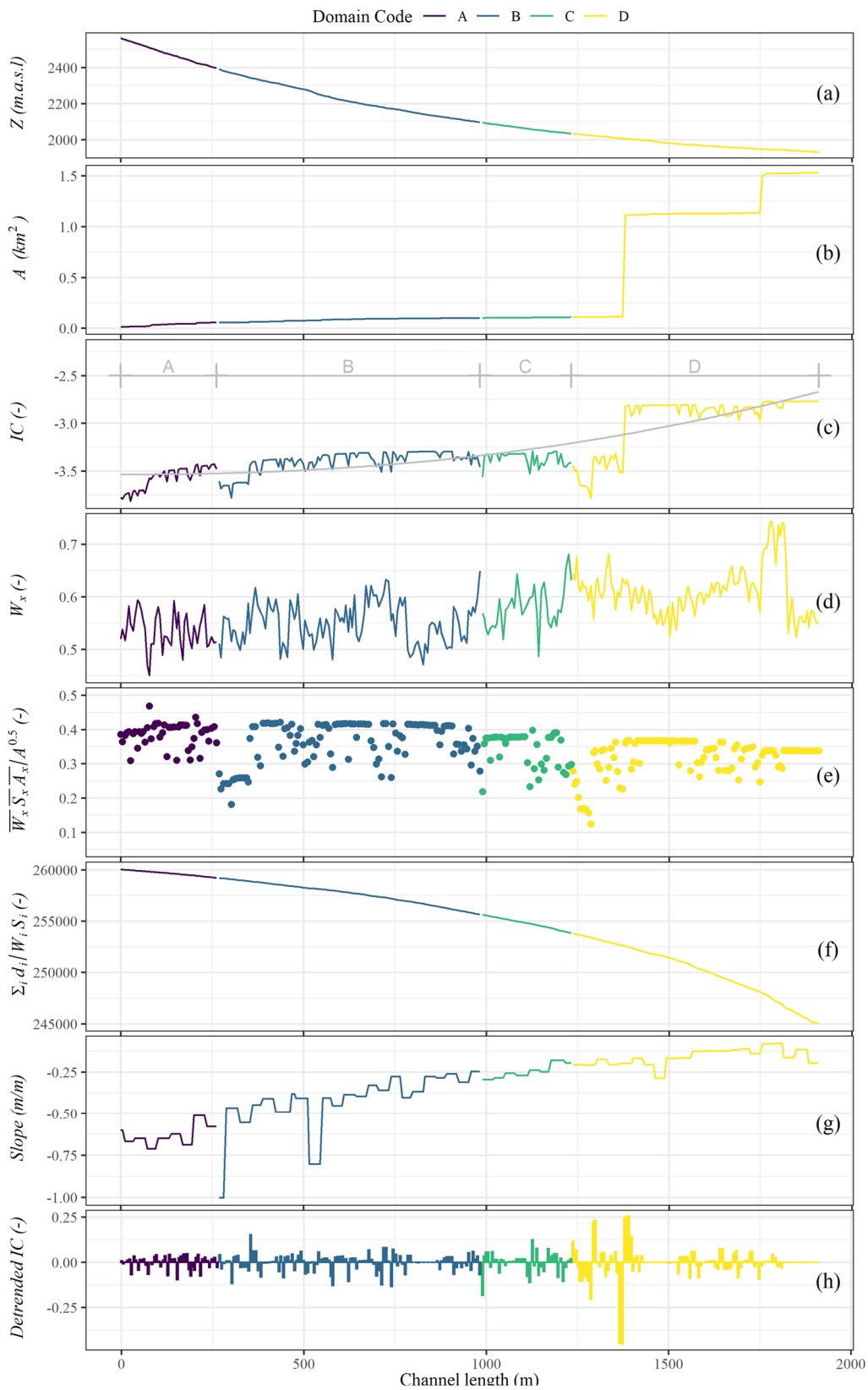


**Fig. 4** Summary plots of the variables that compose IC obtained from the longitudinal analysis application over the 2008 DTM. a) Profile, b) Drainage area, c) IC from literature application, d) Weighting factor, e) Detrended Upslope component (DupDet), f) Downslope component, g) Slope (coef. from the linear model of reaches), h) Detrended IC.

**Table 2** Summary statistics from the analysis of the 2008 and 2018 digital terrain model. Values are expressed as “mean (SD)”.

Domain	Weighting factor		Roughness index (m)		Sediment connectivity index		Slope (m/m)		Sediment budgeting (m <sup>3</sup> /m <sup>2</sup> )	Debris yield rate (m <sup>3</sup> /m)
	2008	2018	2008	2018	2008	2018	2008	2018		
A	0.54 (0.03)	-	0.20 (0.07)	-	-3.58 (0.12)	-	-0.63 (0.06)	-	-	-
B	0.55 (0.04)	0.55 (0.04)	0.17 (0.07)	0.17 (0.08)	-3.40 (0.11)	-3.40 (0.09)	-0.42 (0.16)	-0.46 (0.16)	-1.49 (0.93)	-65.0 (11.6)
C	0.58 (0.04)	0.59 (0.04)	0.12 (0.05)	0.11 (0.09)	-3.37 (0.07)	-3.40 (0.29)	-0.25 (0.04)	-0.30 (0.02)	+0.88 (0.11)	+81.7 (24.5)
D	0.61 (0.05)	-	0.11 (0.09)	-	-2.96 (0.28)	-	-0.16 (0.05)	-	-	-

**Note:** “-”, no data.

same). For the confined domains, the roughness index reports the value of  $0.20 \pm 0.07$  m for domain A and  $0.17 \pm 0.07$  m for domain B. Unconfined areas of the analysed channel show RI values of  $0.12 \pm 0.05$  m for domain C and  $0.09 \pm 0.04$  m for domain D. The last section (Domain E) the W report a value of  $0.61 \pm 0.05$  explaining a smooth surface (pastureland) with a peak above of 0.7 in the final part, where the channel is artificially paved and confluence in the Rio Soial.

To validate the prediction of the 2008 analysis, a longitudinal analysis was also conducted on the 2018 DTM adding the information on the reach-averaged erosion or deposition depth  $\Delta Z$ . The analysis aimed at checking (i) if connectivity/disconnectivity patterns discovered in the 2008 analysis were correlated to the erosion/deposition pattern which would mean that IC is indeed correlated to the actual sediment cascade dynamics, and also if (ii) these patterns were still present in the 2018 landforms and eventually enhanced or attenuated. The analysis of the 2018 dataset also allows an understanding of how the succession of debris flows impacted IC factors. The output is reported in Fig. 5, highlighting changes in relevant areas (Fig. 5c-5d).

Most deposition occurred in Domain C (Fig. 5i), i.e. where the IC and upslope de-trended parameter (Fig. 4c & 4e) were consistently pointed as relatively low as compared to the mean trend of the catchment. Consistently, the IC and underlying parameters were relatively high in the Domain B where most of the erosion occurred. Obviously, the geology, i.e. colluvium, is the other key driver of this observation along with the morphology that is, in a sense described by the IC. These observations validate that the IC, a proxy of the structural connectivity, is correlated to the debris flow dynamics that are described rather as being the result of the functional connectivity.

Comparing the longitudinal profiles with the 2008 data (compare dotted line, i.e. previous values, with continuous lines, i.e. more recent value, in Fig. 5), it is possible to see how disconnectivity is still present, especially in the fan areas (domain C). In addition, drops in both IC and DupDet are more evident in the 2018 dataset when compared to the 2008 analysis. Drops in these two factors indicate an increased disconnection of these areas from the sub-catchment outlet. Another observed phenomenon comparing the two periods is a thalweg avulsion that changed the flow with earlier conjunction with the left-hand watercourse. This is observable by a prior increase of drainage area in domain C (Fig. 5b), as in the 2008 morphology (Fig. 4b). The same is also observed in the classical IC maps (Fig. 3a-3b), where the thalweg shifted to the left.

Table 2 shows how the roughness index (RI) and derived weighting factor (W) did not change significantly in the analysed period (same behaviour since W is directly derived from RI). Fig. 6 reports the density plots for both variables (calculated over all domains) to confirm this observation, highlighting only small and not significant differences. The changes in IC analysed below are thus not only due to these factors but also to other parameters (recall that IC is a log<sub>10</sub> parameter so a drop of one unit of IC requires a one order of magnitude drop of the driving parameters).

### 3.4 Geomorphic and connectivity evolution of the sub-catchment

The availability and comparison of DTMs taken in different epochs enable sediment relocation to be detected and quantified in the study area. The elaboration of a DoD in the analysed sub-catchment (Fig. 7) shows how the channel was affected by moderate

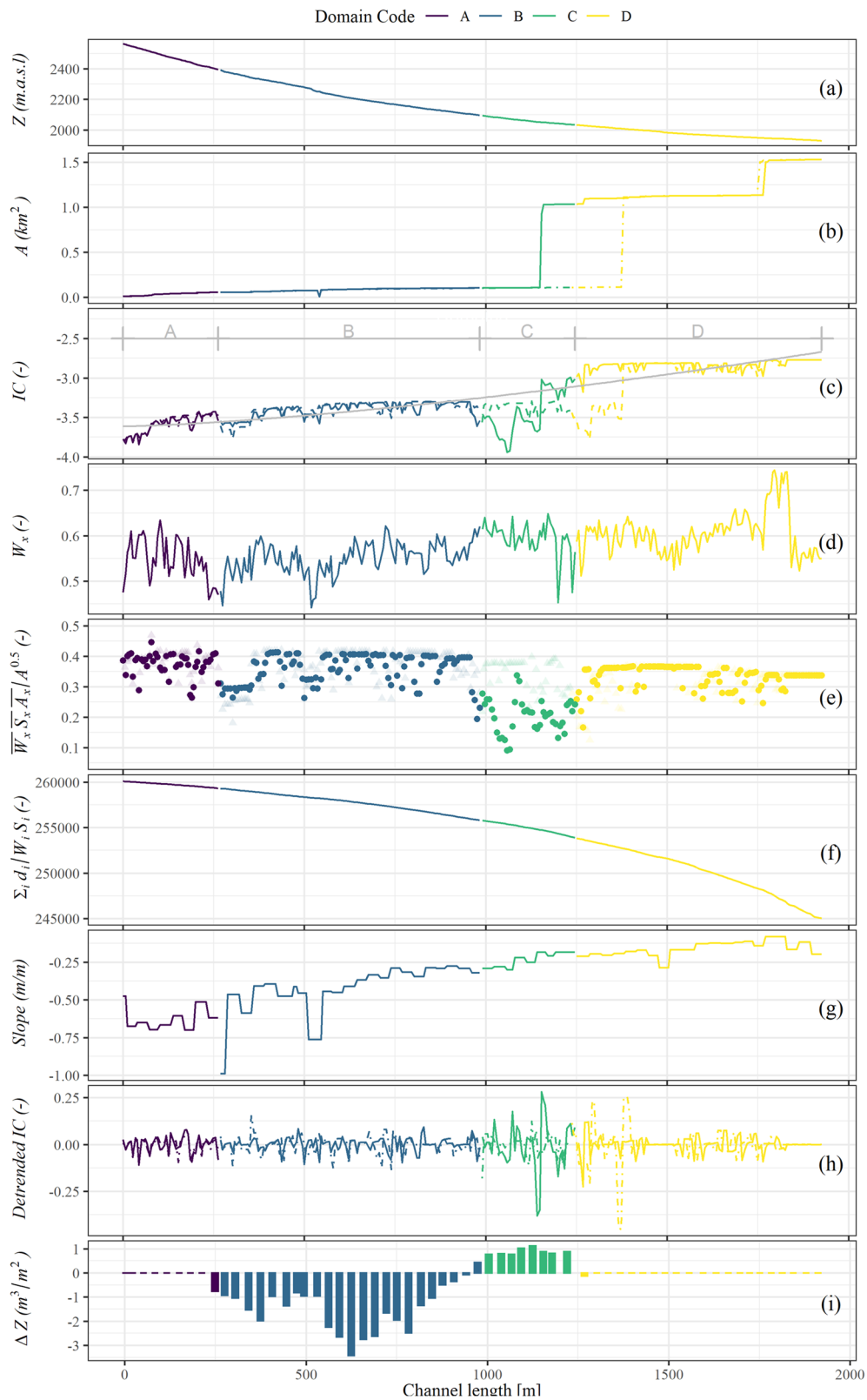


**Fig. 5** Summary plots of the variables that compose IC obtained from the longitudinal analysis application over the 2018 DTM. a) Profile, b) Drainage area, c) IC from literature application, d) Weighting factor, e) Detrended Upslope component (DupDet, f) Downslope component, g)) Slope (coef. from the linear model of reaches, h) Detrended IC, i) sediment budgeting (Net value divided by reach surface). Dotted lines or grey dots display the data of 2008, also shown in Fig. 4 to highlight the changes.

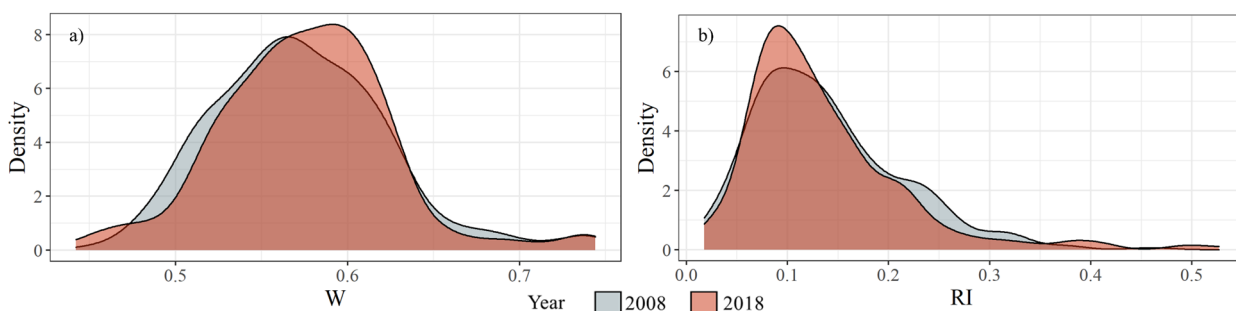


**Fig. 6** Density plots of Weighting factor - W (a) and Roughness Index - RI (b). Variables changes over time are not significant.

to substantial erosion in domain B (Fig. 7b). In this section of the channel, a constant and robust erosion has been observed. Information on volume budgeting is reported in Table 3. The left bank was significantly affected by erosion following the debris flows succession. In the analysed period, the peak of erosion was -9.3 m. The DoD reports a total erosion of  $33,784 \pm 6,096 \text{ m}^3$ , mostly coming from domain B. Dividing the net erosion by the channel area, the unitary erosion rate in domain B is equal to  $-1.49 \pm 0.93 \text{ m}^3/\text{m}^2$ . The fan of the sub-catchment (domain C) is where most of the deposition occurred. The total deposition is about  $22,682 \pm 6,924 \text{ m}^3$  with a unitary deposition rate of  $+0.88 \pm 0.11 \text{ m}^3/\text{m}^2$  (Fig. 7a-7b and Fig. 5i). The sediment budgeting is oriented towards erosion, with a net erosion of  $-11102 \pm 9400 \text{ m}^3$ . Comments on the geomorphic evolution of domains A and D are not possible since the 2018 UAV flight unfortunately did not cover them.

**Table 3** Total volume of erosion and deposition for the thresholded DoD (Difference of DEMs) (minLOD at 0.33 m) between the 2008 and 2018 DTMs.

Domain	Erosion (m <sup>3</sup> )	Deposition (m <sup>3</sup> )
B	$33,325 \pm 5,846$	$1,161 \pm 448$
C	$458 \pm 249$	$21,520 \pm 6,476$
Total	$33,784 \pm 6,096$	$22,682 \pm 6,924$

The cumulated deposition of  $22,682 \text{ m}^3 \pm 6,924 \text{ m}^3$  corresponds to the cumulated geomorphic activity of the five debris flow events that occurred between the two DTM surveys. Reworking by run-off or low-intensity bedload transport is believed to be the main source of the more than  $10,000 \text{ m}^3$  difference between the erosion and deposition. Fine sediment was probably wash out of the area and transported in the downstream river network. Because of the lack of a DTM survey between these debris-flow events, we are unable to highlight the individual effect of each event

and this wash-out. Consequently, the changes in the flow path, topography and sediment connectivity that we highlight here should rather be considered as ongoing trends under low to intermediate magnitude events, than a sudden shift related to one single large magnitude event. Due to the lack of data, we cannot perform several analyses of single events. This would be an interesting topic for further research.

## 4 Discussion

### 4.1 Connectivity Index analysis and prediction capability in a geomorphically changing environment

An integrated understanding of the geomorphic evolution of a debris flow catchment has been pursued through different methods. The application of IC (Fig. 3a and Fig. 3b) produced maps in which the spatial pattern of the index is reported. The analysis of IC maps usually helps to define preferential sediment pathways, which are labelled as “high” or “very high”. The classification of IC maps in seven classes has been performed employing the natural break algorithm (Cucchiario et al. 2019; Tarolli and Sofia 2016). Highly connected areas are usually located within streams and in areas close to the outlet. For example, in the Gardeccia sub-catchment, the confined channels (domains A and B) report higher connectivity since the available energy is condensed along a single preferential path. As reported in the scientific literature (Grimsley et al. 2016), when the confinement degree decrease and flow start spreading, the transport capacity becomes distributed along various flows (highlighted with higher IC values). The flow spreading induced deposition on the fan area (domain C) and in the upper part of domain D.

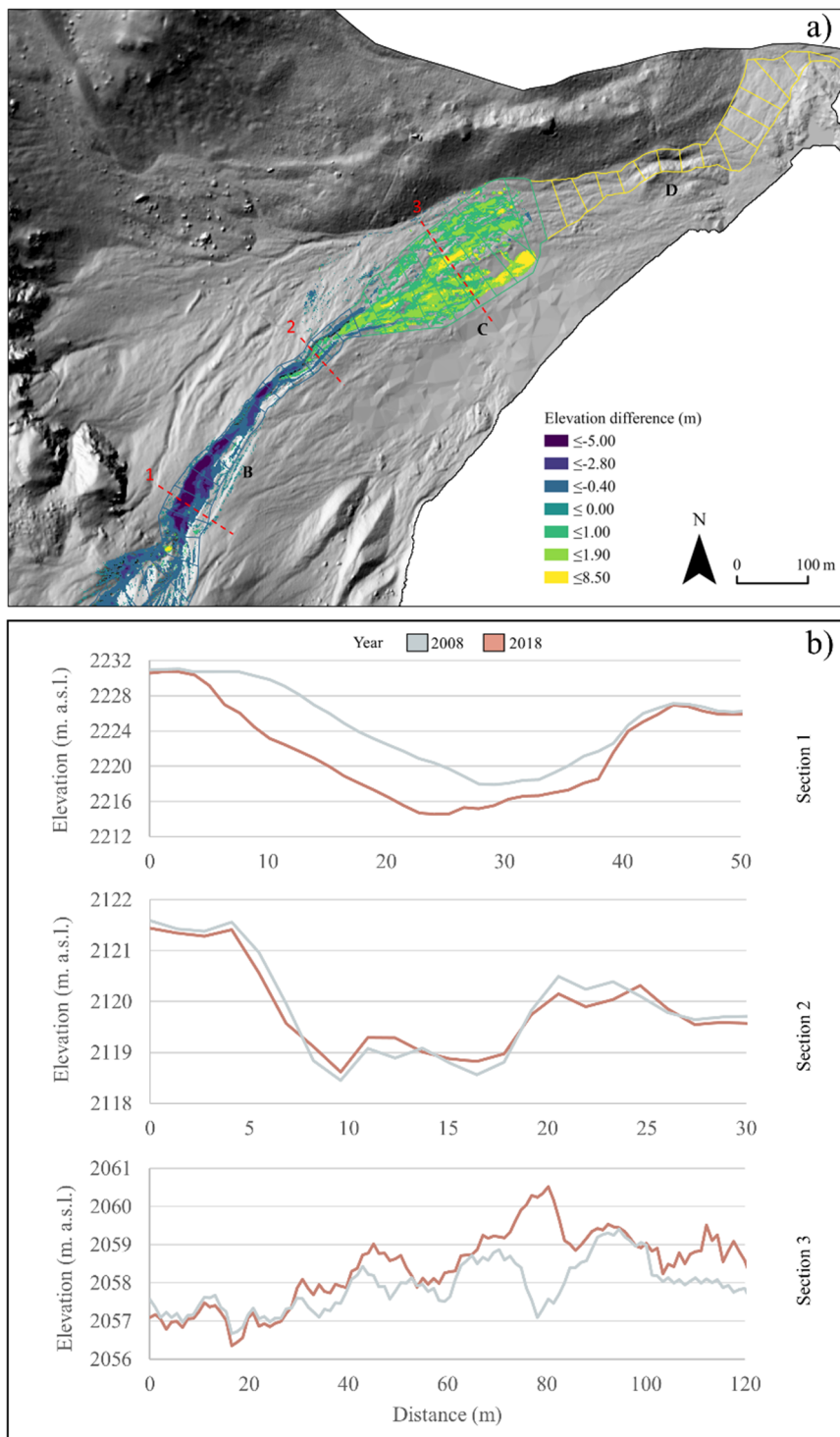


**Fig. 7** (a) Map of the difference between the 2018 and 2008 DEMs of the analysed sub-catchment. The transition between erosion driven dynamics in domain B to deposition in domain C is evident. (b) three representative cross-sections. Section 1 represents diffuse erosion in the upper part of domain B. Section 2 reports an equilibrium between erosion and deposition at the end of domain B, section 3 reports a deposition-oriented pattern in the fan area (domain C).

From qualitative map analysis, it is possible to capture an increased flow spreading in 2018 along

domain C compared to 2008. The spatial distribution of the IC is comparable to the flow accumulation raster, but in this last case, the information about slope, roughness (or other weighting factors), and distance to the target are missing.

Finally, visual interpretation of maps is a powerful tool, but more information can be extracted to evaluate the geomorphic evolution of an area objectively from the IC perspective. While most authors use maps of connectivity indexes, we introduce here a longitudinal analysis of IC and its components to extract more information about the geomorphic features to predict debris flow behaviour from a single DTM. Typically, debris-flow behaviour prediction is based on running several simulations with a numerical tool modelling flow dynamics to get the required information about incision and deposition. Such analyses are however time-consuming and require expertise and good field data. Longitudinal profile analyses are core steps when performing a preliminary geomorphic assessment in a rapidly changing environment, such as a debris flow channel, but it has never been reported by means of the IC index and its composing variables to the best of our knowledge.

By looking at the longitudinal analysis in 2008 and combining Figs. 4c and 4e, the disconnectivity from the model (grey line)

and the decrease in the detrended upslope component (DupDet) explain lower connectivity in the fan area. Furthermore, such values decrease predicts the establishment of deposition dynamics due to flow spreading and channel shifting (as observed from map interpretation).

The prediction of low connectivity is then visible in Fig. 5i, where the sediment budgeting varies gradually from high erosion values in domain B to high values of deposition of domain C. The introduction of the longitudinal analysis confirms the first hypothesis (H1) about the ability to extract more information for detecting disconnectivity in the thalweg and to predict a future sediment erosion/deposition behaviour (Fryirs et al. 2007).

Careful analysis of RI and  $W$  may help identifying the thalweg section where the geomorphic features influence the debris flow behaviour, such as surface smoothing in domain C or rough surface in the confined channel in domain B. The channel incision ranges from about 20 m in the upper section (highly confined) to less than 2 m (at the fan apex). A lower RI combined with poor confinement explains why the flow is more prone to spread in many secondary channels, predicting potential avulsion during future debris-flow events. In domain D, the roughness index tends to decrease, as the surface is smooth and unconfined, and it is where the channel flows through the rangeland near the mountain huts. The flow's confinement is from moderate to low in this reach, driving the weighting factor to relatively high values. Here the depth of the channel is less than 1 m with a shallow slope (Table 1).

The 2018 DTM analyses aim to validate and confirm the predictive capacity of IC, verifying the 2008 outcome. Fig. 5b and 5e, show that the connectivity index decrease (or disconnectivity) still exists and is higher than in 2008. The same is observed in the upslope component pattern, with a prolonged value drops section, confirming decreased connectivity in the fan section. This decrease in the longitudinal analysis captures the flow spreading and channel avulsion in domain C. Evaluating both epochs, it is possible to conclude that the sequence of debris flows and subsequent deposit of material in domain C contributed to increasing this disconnectivity. In this regard, the fan is currently acting as a “non-coupled aggrading fan” (Harvey 2012). While a channel does connect the sub-catchment to Rio Soial, debris-flow events with small to moderate magnitude do not

reach the river and spread material on the fan. Accordingly, from a field survey performed in September 2020, it resulted that the last debris flows triggered by a thunderstorm in July 2019 deposited part of its material in domain C and the lower end of domain B without reaching the sub-catchment outlet.

Finally, the predictive capability of IC (H1) was validated, as also reported in the work of Pellegrini et al. (2021), but with a more profound understanding thanks to the information extracted by the profile analysis.

The multi-temporal evaluation of the RI and  $W$  clearly shows no significant changes (Fig. 6). This indicates that the flow impedance factor has a limited role in IC computation. In practice, flow confinement changes (and eventual distance to the outlet alteration) have a more influential role in estimating connectivity and sediment dynamics.

Provided that the source areas remain very active, no clear water flow will incise a large new channel in the fan, but debris flows will likely continue to spread on it. This means that it is possible to expect more deposition in domain C, meaning a lower sediment volume reaching the pastureland and mountain huts. This can be viewed as an increased disconnection of the fan with the sub-catchment outlet, as reported in comparable cases (Harvey 2012). However, in the context of climate change and related alteration of the rainfall regime and debris flow frequency-magnitude alteration, sediment stored in the channel and on the upper part of the fan could be relocated by a high magnitude debris flow (Blöschl et al. 2019; Hall et al. 2014; Lane et al. 2007).

In the analysed sub-catchment, sediment availability is mainly driven by channel bank failures due to frost-thaw dynamics and splash erosion during intense rainstorms. The sediment recharge rate is relatively fast, and after frequent field surveys, it is possible to define this channel as a “transport limited sub-catchment”.

The IC profile analysis improves the interpretation of a spatially mapped index along the selected channel by adding information about sediment budgeting. In this specific case, the sediment budgeting refers to a quite extended period (ten years), but it is not seen as a limitation since hazard management also accounts for long terms geomorphic evolution to plan the proper mitigation strategies (de Haas et al. 2018; Marchi et al. 2021).

From a practical point of view, mitigation



strategies should favour disconnection in areas where there is space for deposition and restoring connectivity where deposition could be dangerous (Marchi et al. 2019). Needless to say that each intervention should be followed by an accurate study on the consequences to downward areas to avoid channel incision due to an excess of flows available energy.

This work presents an application on a single channel in a small alpine catchment. However, there is the potential to apply the methodology on multiple channels simultaneously or including different variables like numeric model outputs. The IC analysis with the presented methodology is however probably limited to alpine catchments with a drainage area up to 50 km<sup>2</sup>. The reason is also related to the profile analysis of IC, which is not optimal over very wide rivers.

The presented procedure can be easily applied also on a mountain catchment equipped with torrent control works, similarly to the case presented by Cucchiaro et al. (2019). A quantitative profile analysis could help integrate the knowledge derived from the qualitative interpretation of maps and understand in a better way how torrent control works acts on geomorphology and IC (Torresani et al. 2021). Moreover, the longitudinal analysis could be viewed as a data-driven approach requiring less data and less effort to obtain a preliminary scenario before conducting numerical simulation (e.g. 2D dynamics modelling).

The advantage of IC map and IC profile interpretation is that it can be performed easily using a single DTM, allowing a potential prediction of existing disconnection in a defined area of the catchment (or strongly connected sections). For example, deposition in fan areas with low confinement is well known. However, a morphometric index like IC complete interestingly the subjective interpretation of shaded relief images by including at once the information about underlying channel characteristics (distance to the outlet, roughness, drainage area, slope).

#### 4.2 Geomorphic evolution by DTMs differencing

Multiple-epoch high-resolution DTMs are not yet widely available (especially in rural areas or developing countries) since multi-epoch surveys require money and time. We develop a procedure that

exploits a single DTM characterized by a moderate resolution (5 m) through the IC index to make it useful without multi-temporal data.

When available, multi epochs DTMs enable the opportunity to integrate the extracted information by adding a sediment budgeting through a DoD. The DoD computation enabled sediment budgeting to be quantified across the sub-catchment after the recorded debris flows. The results are reported in Fig. 7, Fig. 5i and Table 2 with intense channel erosion predominance in Domain B. Water flowing from domain A (rocky outcrop) is characterised by high available energy and low sediment transport due to the bedrock formation with little sediment availability. When the flow reaches Domain B, erosion starts massively since loose material can be incised, especially from the banks. This dynamic is also known as the “firehose effect” (Curry 1966; Fryxell and Horberg 1943). Domain B is the most eroded part, particularly along the left bank, with elevation changes reaching -9 m. Expressing the sediment budget as debris yield rate (m<sup>3</sup>/m), domain B reports a value of  $-65.0 \pm 11.6$  m<sup>3</sup>/m. This is comparable with literature values for triggering areas with unstable banks and the presence of diffuse loose material (Hungre et al. 1984; Marchi and D’Agostino 2004). A transition from a dominant erosion to a dominant deposition dynamic has been observed in the lower end of domain B. This transition is mainly driven by slope gentling and lowering in confinement degree.

The fan area (domain C) is the part of the sub-catchment where deposition has occurred, with a maximum deposition of about 2.5 m. This is also the domain where deposition dynamics push avulsion and flow spreading to its maximum degree, resulting in the observed 2018 thalweg avulsion to a pre-existing channel. The deposition yield rate here is calculated as  $81.7 \pm 24.5$  m<sup>3</sup>/m.

From an alternative perspective, the longitudinal analysis of Fig. 4i and Fig. 5i reports the DoD values (net value divided by reach surface) to look at how erosion/deposition pattern evolves compared to the IC. These dynamics are also detected in the IC plot (disturbances from the general trend) and the drops in the detrended Upslope component plots. So the second hypothesis (H2) is validated since IC disconnectivity in the fan area is related to deposition driven dynamics, while undisturbed high connectivity in the confined channel is related to high erosion.

Summarising all the results, the integrated

combination of DoD, IC and the longitudinal analysis resulted effective to explain the geomorphic evolution of the sub-catchment after a sequence of debris-flow events and (ii) to exploit hidden information with an alternative point of view.

The open source version of the used R script can be found in (Torresani and Piton 2022) which has then been integrated in the R tool “R\_IC” developed by (Baggio et al. 2022; Martini et al. 2022, with the source code available at- [https://github.com/TommBagg/R\\_IC/releases/tag/R\\_IC\\_v1.0](https://github.com/TommBagg/R_IC/releases/tag/R_IC_v1.0)).

## 5 Conclusion

This investigation aimed to enhance and integrate knowledge on the geomorphic evolution of a dolomitic sub-catchment after a sequence of debris flow events. This was achieved by employing a combination of methods (IC, DoD) and a profile analysis (longitudinal analysis of IC). Along the 10yrs analysed period, the succession of debris flows played a vital role in continuously shaping the morphology of the fan in the sub-catchment, so confirming the high susceptibility to morphology evolution in fan areas (de Haas et al. 2018; Reitz and Jerolmack, 2012). Moreover, it is possible to confirm that both the literature interpretation of IC maps and the longitudinal analysis can capture the same geomorphological behaviour; the latter helping to refine the typical analysis done on debris flow channels. The drops in IC observed in 2008 and increased in 2018 help understand where debris flow starts depositing and that this trend seems to be aggravating.

It was also possible to predict channel evolution from the 2008 longitudinal analysis by comparing the results of the 2018 dataset analysis. The analysis of the 2018 dataset and later field visits confirmed the lack of connectivity in fan areas observed in the 2008 dataset. As the disconnectivity tendencies were confirmed, it is possible to expect more deposition and autogenic avulsion in the fan area, potentially reducing the volume to the downstream grazing land during moderate magnitude events. Of course, this tendency could be overturned by extreme debris flow events or alterations in the magnitude-frequency relationship due to climate change.

Finally, we tested and proved that the combination of the used methodologies can pursue

more advanced knowledge on the mid-term evolution of a sub-catchment in the Dolomites. This tool could be helpful to researchers, professionals and local administrations who need a fast tool to exploit IC in debris flow prone catchment, and to obtain a better understanding on areas where hazard mitigation strategies are under evaluation. Such tool quickly highlights the most connected areas to the outlet and the probable paleo-channels that can be re-activated by a sequence of debris flows.

## Acknowledgements

The authors would like to thank the “Ufficio Sistemi Informativi - Servizio autorizzazioni e valutazioni ambientali” of the Autonomous Province of Trento for providing the LIDAR derived DTM from the flights performed in 2006/2007/2008 (<http://www.territorio.provincia.tn.it/portal/server.pt/community/lidar/847/lidar/23954>). A special thanks also to the Authority for mountain basins of the Autonomous Province of Trento (Servizio Bacini Montani), mainly to Ruggero Valentinotti and Dr Gabriele Bertoldi, for the support in choosing the Gardeccia study area and for the logistic support on the first phases of the study. A special thanks also to the local police unit of Sèn Jan di Fassa municipality and its Major (Giulio Florian) for issuing the pass to access the study area. This paper was improved by the numerous comments of five reviewer on the previous versions.

## Open Access

This article is licensed under a Creative Commons Attribution 4.0 International License, which permits use, sharing, adaptation, distribution and reproduction in any medium or format, as long as you give appropriate credit to the original author(s) and the source, provide a link to the Creative Commons license, and indicate if changes were made. The images or other third party material in this article are included in the article’s Creative Commons license, unless indicated otherwise in a credit line to the material. If material is not included in the article’s Creative Commons license and your intended use is not permitted by statutory regulation or exceeds the permitted use, you will need to obtain permission directly from the copyright holder. To view a copy of this license,

visit <http://creativecommons.org/licenses/by/4.0/>.

Open access funding provided by Università degli

Studi di Padova within the CRUI-CARE Agreement.

## References

- Agiuera-Vega F, Carvajal-Ramírez F, Martínez-Carricondo P, et al. (2018) Reconstruction of extreme topography from UAV structure from motion photogrammetry. *Measurement* 121: 127-138. <https://doi.org/10.1016/J.MEASUREMENT.2018.02.062>
- Baggio T, Martini L, Torresani L (2022) R\_IC\_v1.0. <https://doi.org/10.5281/ZENODO.6566013>
- Benda L, Veldhuisen C, Black J (2003) Debris flows as agents of morphological heterogeneity at low-order confluences, Olympic Mountains, Washington. *Bull Geol Soc Am* 115: 1110-1121. <https://doi.org/10.1130/B25265.1>
- Blöschl G, Hall J, Viglione A, et al. (2019) Changing climate both increases and decreases European river floods. *Nature* 573: 108-111. <https://doi.org/10.1038/s41586-019-1495-6>
- Borselli L, Cassi P, Torri D (2008) Prolegomena to sediment and flow connectivity in the landscape: A GIS and field numerical assessment. *Catena* 75: 268-277. <https://doi.org/10.1016/j.catena.2008.07.006>
- Bovis MJ, Jakob M (1999) The role of debris supply conditions in predicting debris flow activity. *Earth Surf Process Landforms* 24: 1039-1054. [https://doi.org/10.1002/\(SICI\)1096-9837\(199910\)24:11<1039::AID-ESP29>3.0.CO;2-U](https://doi.org/10.1002/(SICI)1096-9837(199910)24:11<1039::AID-ESP29>3.0.CO;2-U)
- Brierley G, Fryirs K, Jain V (2006) Landscape connectivity: The geographic basis of geomorphic applications. *Area* 38: 165-174. <https://doi.org/10.1111/j.1475-4762.2006.00671.x>
- Cavalli M, Goldin B, Comiti F, et al. (2017) Assessment of erosion and deposition in steep mountain basins by differencing sequential digital terrain models. *Geomorphology* 291: 4-16. <https://doi.org/10.1016/j.geomorph.2016.04.009>
- Cavalli M, Tarolli P, Marchi L, et al. (2008) The effectiveness of airborne LiDAR data in the recognition of channel-bed morphology. *Catena* 73: 249-260. <https://doi.org/10.1016/j.catena.2007.11.001>
- Cavalli M, Trevisani S, Comiti F, et al. (2013) Geomorphometric assessment of spatial sediment connectivity in small Alpine catchments. *Geomorphology* 188: 31-41. <https://doi.org/10.1016/j.geomorph.2012.05.007>
- Costa JE, Williams GP (1984) Debris-flow dynamics, Open-File Report. <https://doi.org/10.3133/OFR84606>
- Crema S, Cavalli M (2018) SedInConnect: a stand-alone, free and open source tool for the assessment of sediment connectivity. *Comput Geosci* 111: 39-45. <https://doi.org/10.1016/j.cageo.2017.10.009>
- Cucchiari S, Cazorzi F, Marchi L, et al. (2019) Multi-temporal analysis of the role of check dams in a debris-flow channel: Linking structural and functional connectivity. *Geomorphology* 345: 106844. <https://doi.org/10.1016/j.geomorph.2019.106844>
- Curry RR (1966) Observation of alpine mudflows in the Tenmile range, central Colorado. *Bull Geol Soc Am* 77: 771-776. [https://doi.org/10.1130/0016-7606\(1966\)77\[771:OOAMIT\]2.0.CO;2](https://doi.org/10.1130/0016-7606(1966)77[771:OOAMIT]2.0.CO;2)
- D'Agostino V, Bertoldi G (2014) On the assessment of the management priority of sediment source areas in a debris-flow catchment. *Earth Surf Process Landforms* 39: 656-668. <https://doi.org/10.1002/esp.3518>
- de Haas T, Kruijt A, Densmore AL (2018) Effects of debris-flow magnitude-frequency distribution on avulsions and fan development. *Earth Surf Process Landforms* 43: 2779-2793. <https://doi.org/10.1002/esp.4432>
- De Haas T, Van Den Berg W, Braat L, et al. (2016) Autogenic avulsion, channelization and backfilling dynamics of debris-flow fans. *Sedimentology* 63: 1596-1619. <https://doi.org/10.1111/sed.12275>
- Fryirs K (2013) (Dis)Connectivity in catchment sediment cascades: A fresh look at the sediment delivery problem. *Earth Surf Process Landforms* 38: 30-46. <https://doi.org/10.1002/esp.3242>
- Fryirs KA, Brierley GJ, Preston NJ, et al. (2007) Buffers, barriers and blankets: The (dis) connectivity of catchment-scale sediment cascades. *Catena* 70: 49-67. <https://doi.org/10.1016/j.catena.2006.07.007>
- Fryxell FM, Horberg L (1943) Alpine mudflows in Grand Teton National Park, Wyoming. *Bull Geol Soc Am* 54: 457-472. <https://doi.org/10.1130/GSAB-54-457>
- Ghuffar S (2018) DEM Generation from multi satellite PlanetScope imagery. *Remote Sens* 10: 1462. <https://doi.org/10.3390/rs10091462>
- Gregoretto C, Stancanelli LM, Bernard M, et al. (2019) Relevance of erosion processes when modelling in-channel gravel debris flows for efficient hazard assessment. *J Hydrol* 568: 575-591. <https://doi.org/10.1016/j.jhydrol.2018.10.001>
- Grimsley KJ, Rathburn SL, Friedman JM, et al. (2016) Debris Flow Occurrence and Sediment Persistence, Upper Colorado River Valley, CO. *Environ Manage* 58: 76-92. <https://doi.org/10.1007/s00267-016-0695-1>
- Hall J, Arheimer B, Borga M, et al. (2014) Understanding flood regime changes in Europe: A state-of-the-art assessment. *Hydrol Earth Syst Sci* 18: 2735-2772. <https://doi.org/10.5194/hess-18-2735-2014>
- Harvey AM (2012) The coupling status of alluvial fans and debris cones: A review and synthesis. *Earth Surf Process Landforms*. <https://doi.org/10.1002/esp.2213>
- Harvey AM (2001) Coupling between hillslopes and channels in upland fluvial systems: Implications for landscape sensitivity, illustrated from the Howgill Fells, northwest England. *Catena* 42: 225-250. [https://doi.org/10.1016/S0341-8162\(00\)00139-9](https://doi.org/10.1016/S0341-8162(00)00139-9)
- Heckmann T, Cavalli M, Cerdan O, et al. (2018) Indices of sediment connectivity: opportunities, challenges and limitations. *Earth-Science Rev*. <https://doi.org/10.1016/j.earscirev.2018.08.004>
- Heckmann T, Schwanghart W (2013) Geomorphic coupling and sediment connectivity in an alpine catchment - Exploring sediment cascades using graph theory. *Geomorphology* 182: 89-103. <https://doi.org/10.1016/j.geomorph.2012.10.033>
- Hengl T (2006) Finding the right pixel size. *Comput Geosci* 32: 1283-1298. <https://doi.org/10.1016/j.cageo.2005.11.008>
- Hungr O, Morgan GC, Kellerhals R (1984) Quantitative analysis of debris torrent hazards for design of remedial measures. *Can Geotech J* 21: 663-677. <https://doi.org/10.1139/t84-073>
- Kaitna R, Huebl J (2013) Silent Witnesses for Torrential Processes, in: *Advances in Global Change Research*. Springer International Publishing, pp 111-130. [https://doi.org/10.1007/978-94-007-4336-6\\_7](https://doi.org/10.1007/978-94-007-4336-6_7)
- Korup O, Densmore AL, Schlunegger F (2010) The role of landslides in mountain range evolution. *Geomorphology* 120: 77-90. <https://doi.org/10.1016/j.geomorph.2009.09.017>
- Kumar A, Bhambri R, Tiwari SK, et al. (2019) Evolution of debris flow and moraine failure in the Gangotri Glacier region, Garhwal Himalaya: Hydro-geomorphological aspects. *Geomorphology* 333: 152-166.

- <https://doi.org/10.1016/j.geomorph.2019.02.015>  
 Lane SN (2013) 21st century climate change: Where has all the geomorphology gone? *Earth Surf Process Landforms*.  
<https://doi.org/10.1002/esp.3362>
- Lane SN, Tayefi V, Reid SC, et al. (2007) Interactions between sediment delivery, channel change, climate change and flood risk in a temperate upland environment. *Earth Surf. Process. Landforms* 32: 429-446.  
<https://doi.org/10.1002/esp.1404>
- Llena M, Vericat D, Cavalli M, et al. (2019) The effects of land use and topographic changes on sediment connectivity in mountain catchments. *Sci Total Environ* 660: 899-912.  
<https://doi.org/10.1016/j.scitotenv.2018.12.479>
- López-Vicente M, Ben-Salem N (2019) Computing structural and functional flow and sediment connectivity with a new aggregated index: A case study in a large Mediterranean catchment. *Sci Total Environ* 651: 179-191.  
<https://doi.org/10.1016/j.scitotenv.2018.09.170>
- López-Vicente M, Quijano L, Palazón L, et al. (2015) Assessment of soil redistribution at catchment scale by coupling a soil erosion model and a sediment connectivity index (central Spanish pre-pyrenees). *Cuad Investig Geográfica* 41: 127.  
<https://doi.org/10.18172/cig.2649>
- Mao L, Cavalli M, Comiti F, et al. (2009) Sediment transfer processes in two Alpine catchments of contrasting morphological settings. *J Hydrol* 364: 88-98.  
<https://doi.org/10.1016/j.jhydrol.2008.10.021>
- Marchi L, Cazorzi F, Arattano M, et al. (2021) Debris flows recorded in the Moscardo catchment (Italian Alps) between 1990 and 2019. *Nat Hazards Earth Syst Sci* 21: 87-97.  
<https://doi.org/10.5194/nhess-21-87-2021>
- Marchi L, Comiti F, Crema S, et al. (2019) Channel control works and sediment connectivity in the European Alps. *Sci Total Environ* 668: 389-399.  
<https://doi.org/10.1016/j.scitotenv.2019.02.416>
- Marchi L, D'Agostino V (2004) Estimation of debris-flow magnitude in the Eastern Italian Alps. *Earth Surf Process Landforms* 29: 207-220.  
<https://doi.org/10.1016/j.jhydrol.2004.10.021>
- Martini L, Baggio T, Torresani L, et al. (2022) R\_IC: A novel and versatile implementation of the index of connectivity in R. *Environ Model Softw* 155.  
<https://doi.org/10.1016/j.envsoft.2022.105446>
- Martini L, Faes L, Picco L, et al. (2020) Assessing the effect of fire severity on sediment connectivity in central Chile. *Sci Total Environ* 728: 139006.  
<https://doi.org/10.1016/j.scitotenv.2020.139006>
- Masselink RJH, Keesstra SD, Temme AJAM, et al. (2016) Modelling Discharge and Sediment Yield at Catchment Scale Using Connectivity Components. *L Degrad Dev* 27: 933-945.  
<https://doi.org/10.1002/ldr.2512>
- Messenzehl K, Hoffmann T, Dikau R (2014) Sediment connectivity in the high-alpine valley of Val Mütschans, Swiss National Park - linking geomorphic field mapping with geomorphometric modelling. *Geomorphology* 221: 215-229.  
<https://doi.org/10.1016/j.geomorph.2014.05.033>
- Najafi S, Dragovich D, Heckmann T, Sadeghi SH (2021) Sediment connectivity concepts and approaches. *Catena*.  
<https://doi.org/10.1016/j.catena.2020.104880>
- O'Brien GR, Wheaton JM, Fryirs K, et al. (2019) Mapping valley bottom confinement at the network scale. *Earth Surf Process Landforms* 44:1828-1845.  
<https://doi.org/10.1002/esp.4615>
- Ortiz-Rodríguez AJ, Borselli L, Sarocchi D (2017) Flow connectivity in active volcanic areas: Use of index of connectivity in the assessment of lateral flow contribution to main streams. *Catena* 157: 90-111.  
<https://doi.org/10.1016/j.catena.2017.05.009>
- Pellegrini G, Martini L, Cavalli M, et al. (2021) The morphological response of the Tegnás alpine catchment (Northeast Italy) to a Large Infrequent Disturbance. *Sci Total Environ* 770: 145209.  
<https://doi.org/10.1016/j.scitotenv.2021.145209>
- Reitz MD, Jerolmack DJ (2012) Experimental alluvial fan evolution: Channel dynamics, slope controls, and shoreline growth. *J Geophys Res Earth Surf* 117: F02021.  
<https://doi.org/10.1029/2011JF002261>
- Rinaldi M, Piégay H, Surian N (2011) Geomorphological Approaches for River Management and Restoration in Italian and French Rivers. *core.ac.uk*.  
<https://doi.org/10.1029/2010GM000984>
- Roux C, Alber A, Bertrand M, et al. (2015) "FluvialCorridor": A new ArcGIS toolbox package for multiscale riverscape exploration. *Geomorphology* 242: 29-37.  
<https://doi.org/10.1016/j.geomorph.2014.04.018>
- Schneuwly-Bollschweiler M, Stoffel M (2012) Hydrometeorological triggers of periglacial debris flows in the Zermatt valley (Switzerland) since 1864. *J Geophys Res Earth Surf* 117. <https://doi.org/10.1029/2011JF002262>
- Schopper N, Mergili M, Frigerio S, et al. (2019) Analysis of lateral sediment connectivity and its connection to debris flow intensity patterns at different return periods in the Fella River system in northeastern Italy. *Sci Total Environ* 658: 1586-1600. <https://doi.org/10.1016/j.scitotenv.2018.12.288>
- Takahashi T (1981) Debris Flow. *Annu Rev Fluid Mech* 13: 57-77.  
<https://doi.org/10.1146/annurev.fl.13.010181.000421>
- Tarboton DG (1997) A new method for the determination of flow directions and upslope areas in grid digital elevation models. *Water Resour Res* 33: 309-319.  
<https://doi.org/10.1029/96WR03137>
- Tarolli P (2014) High-resolution topography for understanding Earth surface processes: Opportunities and challenges. *Geomorphology*.  
<https://doi.org/10.1016/j.geomorph.2014.03.008>
- Tarolli P, Sofia G (2016) Human topographic signatures and derived geomorphic processes across landscapes. *Geomorphology* 255: 140-161.  
<https://doi.org/10.1016/j.geomorph.2015.12.007>
- Torresani L, D'Agostino V, Piton G (2021) Deciphering sediment Connectivity Index and erosion pattern in a debris flow catchment, in: 14th INTERPRAEVENT Congress: Natural Hazards in a Changing World. International Research Society INTERPRAEVENT, Bergen (virtual), Norway. pp 303-311.
- Torresani L, Piton G (2022) IC profile analysis V.1.0.  
<https://doi.org/10.5281/ZENODO.5905877>
- Trevisani S, Cavalli M (2016) Topography-based flow-directional roughness: Potential and challenges. *Earth Surf Dyn* 4: 343-358. <https://doi.org/10.5194/esurf-4-343-2016>
- Ufficio Sistemi Informativi - Servizio autorizzazioni e valutazioni ambientali (2009) Caratteristiche rilievo lidar (lidar survey characteristics).
- Wheaton JM, Brasington J, Darby SE, et al. (2010) Accounting for uncertainty in DEMs from repeat topographic surveys: Improved sediment budgets. *Earth Surf Process Landforms* 35: 136-156. <https://doi.org/10.1002/esp.1886>
- Williams RD (2012) DEMs of Difference. *Geomorphol. Tech.* 2, 1-17.
- Zanandrea F, Michel GP, Kobiyama M (2020) Impedance influence on the index of sediment connectivity in a forested mountainous catchment. *Geomorphology* 351.  
<https://doi.org/10.1016/j.geomorph.2019.106962>
- Zhao G, Gao P, Tian P, et al. (2020) Assessing sediment connectivity and soil erosion by water in a representative catchment on the Loess Plateau, China. *Catena* 185: 104284.  
<https://doi.org/10.1016/j.catena.2019.104284>